American Mineralogist, Volume 80, pages 387–393, 1995

The crystal structure of manandonite-$2H_2$

HONG ZHENG,* STURGES W. BAILEY†
Department of Geology and Geophysics, University of Wisconsin, 1215 West Dayton Street, Madison, Wisconsin 53706, U.S.A.

ABSTRACT

The crystal structure of manandonite-$2H_2$, an Al-, Li-, B-rich analogue of amesite, has been refined in space group $C1$ to $R = 5.7\%$. Tetrahedral Si, Al, and B are partly ordered to give two mean T-O bond lengths near 1.603(1) Å and two near 1.667(1) Å. B has a greater tendency to order than do Si and Al. There are one relatively Li-rich octahedron and two relatively Al-rich octahedra in each layer with mean M-O,OH bond lengths of 1.997(1), 1.960(1), and 1.955(1) Å, respectively, in layer 1 and 2.014(1), 1.941(1), and 1.956(1) Å, respectively, in layer 2. It is the partial ordering of the octahedral cations that decreases the ideal $P6_3$ symmetry to $P1$ (or $C1$, as used for refinement). Tetrahedral rotations of 18.3° are required to match the larger lateral dimensions of the tetrahedral sheet with those of the octahedral sheet, coupled with basal O corrugations because of the different sizes of the octahedra. The H^+ protons of the six surface OH molecules point directly toward their acceptor basal O atoms to give H bond contacts between 2.647 and 2.773 Å.

INTRODUCTION

Lacroix (1912, 1922) described manandonite as an Al-, Li-, and B-rich phyllosilicate occurring as nearly white platelets with sixfold sector twins on (001). The material occurs in the Li-, B-, and Mn-rich Antandrokomby pegmatite on the bank of the Manandona River near Antsirabe in Madagascar. An Al-, Li-, and B-rich chlorite is also present and was mistaken for manandonite by Strunz (1957). As a result, there are several references to manandonite in the later literature as B-rich cookeite (Frank-Kamenetsky, 1960; Sahama et al., 1968; Caillère et al., 1982; Hawthorne and Černý, 1982; London and Burt, 1982; Fleischer, 1987). Ranorosoa et al. (1989) reinvestigated specimens from the type locality and proved that the material described by Lacroix has a 1:1 structure of ideal composition $(Al_2Li)(SiAl_{0.5}B_{0.5})O_5(OH)_4$. It occurs as the $2H_2$ polytype of Bailey (1969) and can be considered as an Al-, Li-, and B-rich analogue of amesite, $(Mg_2Al)(SiAl)O_5(OH)_4$. Chemical analysis of hand-picked material by Ranorosoa et al. (1989) yielded a formula unit of $(Al_{2.016}Li_{0.936}Mg_{0.002}Mn_{0.002})_{2.956}(Si_{0.997}Al_{0.427}B_{0.576})O_5(OH)_4$, neglecting small amounts of Na and Ca (0.01 atoms each).

Crystals of manandonite were kindly sent to us by A.-M. Fransolet (Université de Liège, Belgium) for the purpose of structural refinement. The observation of biaxial sixfold sector twins on (001) and the overall similarity of manandonite to amesite suggest that cation ordering has reduced the ideal hexagonal symmetry ($P6_3$) of the $2H_2$ polytype. Ranorosoa et al. (1989) reported the extinction rules as consistent with orthorhombic space group $C222_1$. But the $l = 2n + 1$ absences observed for $00l$ reflections are structural absences due to the similarities of the two layers in the structure, rather than due to a twofold screw axis, and a triclinic space group of $C1$ is more likely (as in amesite-$2H_2$).

Two ordering patterns of the tetrahedral and octahedral cations were determined in different specimens of triclinic amesite-$2H_2$ by Hall and Bailey (1979) and Anderson and Bailey (1981). The latter authors showed that there are seven unique ordering patterns that are theoretically possible for amesite-$2H_2$, and even more patterns are possible in manandonite-$2H_2$ if $^{[4]}$Si, $^{[4]}$Al, and $^{[4]}$B order into separate tetrahedra. Ordering of three tetrahedral elements requires different tetrahedral compositions for the two layers of the C-centered orthohexagonal unit used for the $2H_2$ structure, development of a lateral superlattice, or the loss of C centering. In addition, the favored ordering patterns in manandonite can be expected to be different from those in amesite because of the different ratios of large and small octahedral cations and their differing charges. Amesite has two large Mg^{2+} and one small Al^{3+} cation present in the three octahedra of each layer, whereas manandonite has one large Li^{1+} and two small Al^{3+} cations in each layer.

The purposes of this study were to (1) examine the effect of $^{[4]}$B on ordering, (2) determine the ordering pattern and analyze it relative to the patterns observed in the amesite structures, (3) analyze the structural distortions occurring as a result of the different sizes and charges of the ordered cations relative to amesite, and (4) determine the positions of the H^+ protons of the OH groups.

* Present address: 8109 West 96th Street, Bloomington, Minnesota 55438, U.S.A.
† Deceased November 30, 1994.

0003–004X/95/0304–0387$02.00

TABLE 1. Atomic positions and anisotropic displacement parameters

Atom	x	y	z	U_{11}	U_{22}	U_{33}	U_{23}	U_{13}	U_{12}	U_{eq}
M1	0.1693(3)	0.1705(3)	0.2250(2)	0.0245(5)	0.0319(8)	0.0365(4)	0.0018(8)	−0.0026(8)	0.0076(8)	0.0310(1)
M2	0.6770(4)	0.0003(3)	0.2256(2)	0.0265(5)	0.0320(7)	0.0334(6)	0.0014(5)	0.0020(2)	0.0069(9)	0.0306(1)
M3	0.6739(4)	0.3347(3)	0.2247(3)	0.0273(5)	0.0378(8)	0.0325(4)	−0.0028(5)	−0.0011(2)	0.0073(8)	0.0325(2)
T1	0.0120(4)	0.0002(3)	0.0298(2)	0.0084(6)	0.0279(9)	0.0848(8)	−0.0027(3)	−0.0057(1)	0.0122(6)	0.0404(2)
T2	0.0149(4)	0.3328(4)	0.0298(2)	0.0303(6)	0.0470(9)	0.0558(8)	0.0044(2)	−0.0033(2)	0.0063(3)	0.0444(2)
O1	0.0099(4)	0.0006(4)	0.1506(3)	0.0201(7)	0.0347(7)	0.0377(7)	0.0018(9)	−0.0027(5)	0.0043(3)	0.0308(2)
O2	0.0166(4)	0.3345(3)	0.1456(3)	0.0237(7)	0.0293(7)	0.0310(8)	0.0000(7)	−0.0025(4)	0.0060(5)	0.0280(2)
O3	0.1109(3)	0.1703(3)	−0.0097(2)	0.0863(7)	0.0825(8)	0.0877(6)	0.0109(3)	0.0055(5)	−0.0081(5)	0.0855(6)
O4	0.2106(4)	0.4612(4)	−0.0114(2)	0.0797(7)	0.0902(8)	0.0935(8)	0.0014(3)	−0.0079(7)	−0.0005(3)	0.0878(7)
O5	0.2212(4)	−0.1332(4)	−0.0096(2)	0.1020(8)	0.0990(9)	0.0961(7)	−0.0067(5)	0.0014(6)	0.0117(3)	0.0990(8)
OH1	0.5106(4)	0.1632(4)	0.1498(2)	0.0235(6)	0.0347(7)	0.0354(9)	−0.0016(5)	−0.0008(4)	0.0069(6)	0.0312(2)
OH2	0.3458(5)	0.0099(4)	0.2936(3)	0.0381(6)	0.0343(7)	0.0234(8)	−0.0043(4)	0.0003(2)	0.0055(2)	0.0319(2)
OH3	0.3385(4)	0.3392(4)	0.2954(3)	0.0338(8)	0.0298(7)	0.0245(8)	0.0008(6)	−0.0006(7)	0.0093(8)	0.0294(2)
OH4	0.8489(4)	0.1665(3)	0.2977(2)	0.0300(9)	0.0415(7)	0.0236(8)	−0.0034(3)	0.0017(6)	0.0009(9)	0.0317(2)
M11	0.3377(4)	0.3244(3)	0.7244(2)	0.0187(3)	0.0331(7)	0.0372(8)	−0.0038(6)	−0.0000(8)	0.0160(8)	0.0297(2)
M22	−0.1612(4)	0.4972(3)	0.7261(3)	0.0192(4)	0.0285(6)	0.0299(8)	0.0004(2)	−0.0036(5)	0.0127(9)	0.0259(1)
M33	−0.1556(4)	0.1633(3)	0.7265(3)	0.0173(4)	0.0282(6)	0.0296(7)	0.0004(7)	0.0019(2)	0.0144(2)	0.0250(1)
T11	0.0131(4)	−0.0011(3)	0.5305(2)	0.0367(5)	0.0453(6)	0.0671(7)	0.0049(3)	−0.0064(3)	0.0128(8)	0.0497(2)
T22	−0.4889(4)	0.1630(3)	0.5304(2)	0.0249(4)	0.0337(9)	0.0700(6)	0.0014(5)	−0.0079(1)	0.0162(7)	0.0429(2)
O11	0.0218(4)	0.0044(3)	0.6517(3)	0.0576(6)	0.0585(9)	0.0499(6)	−0.0024(5)	−0.0006(4)	0.0077(2)	0.0553(3)
O22	−0.4891(4)	0.1563(3)	0.6464(3)	0.0501(6)	0.0488(8)	0.0448(5)	−0.0016(2)	0.0004(7)	0.0068(4)	0.0479(2)
O33	0.3134(4)	0.0367(3)	0.4874(2)	0.0948(7)	0.0926(7)	0.0970(6)	−0.0032(5)	0.0042(6)	−0.0014(9)	0.0948(7)
O44	−0.5873(4)	0.3272(4)	0.4948(2)	0.1088(6)	0.1015(8)	0.1057(7)	−0.0019(3)	−0.0082(4)	0.0033(7)	0.1053(7)
O55	−0.1970(4)	0.1310(3)	0.4907(2)	0.1067(5)	0.1118(8)	0.1066(9)	0.0062(8)	0.0032(5)	0.0031(4)	0.1097(7)
OH11	0.0032(4)	0.3302(2)	0.6500(2)	0.0503(7)	0.0400(9)	0.0382(8)	0.0004(3)	0.0010(5)	0.0072(1)	0.0428(2)
OH22	−0.3176(3)	0.3230(4)	0.7943(3)	0.0255(7)	0.0304(9)	0.0275(9)	0.0033(3)	0.0022(6)	0.0109(2)	0.0278(2)
OH33	0.1619(3)	0.4945(4)	0.7945(3)	0.0254(6)	0.0409(9)	0.0234(7)	0.0054(2)	−0.0031(8)	0.0045(2)	0.0299(2)
OH44	0.1686(4)	0.1556(4)	0.7996(2)	0.0239(5)	0.0313(8)	0.0289(7)	0.0005(7)	0.0000(5)	0.0076(9)	0.0280(1)
H1	0.5271	0.1890	0.0894							
H2	0.3193	0.0192	0.3589							
H3	0.3639	0.3464	0.3606							
H4	0.8268	0.1550	0.3621							
H11	0.9866	0.3046	0.5903							
H22	0.6961	0.3379	0.8601							
H33	0.6895	0.9835	0.8598							
H44	0.1443	0.1645	0.8648							

EXPERIMENTAL METHODS AND REFINEMENT

No evidence for a lateral superlattice was found during preliminary X-ray study of manandonite crystals, and no odd orders of the 00l reflections were recorded. We considered the possibility of the loss of C centering by collecting a complete data set of intensities using a primitive cell. No violations of C centering were found, and so it is not likely that complete ordering of Si, Al, and B into separate tetrahedral sites has occurred. The structure was refined as $C1$, as for the amesite-2H_2 structures. In the 2H_2 structure there is an alternation of $-b/3$ and $+b/3$ shifts of the sixfold rings between adjacent layers, as well as alternation of the occupation of the two possible sets of octahedral cation positions (I and II). We use an orientation of the structure with layer 2 shifted by $-b/3$ relative to layer 1. Set II of octahedral positions is occupied in layer 1, and set I in layer 2.

A rectangular crystal 0.32 × 0.28 mm on the edges and 0.02 mm thick (University of Wisconsin Geological Museum no. 6003/4) was used for data collection on a Siemens P4RA single-crystal diffractometer. Unit-cell parameters of a = 5.070(1), b = 8.776(2), c = 13.778(3) Å, α = 90.09(2), β = 90.12(2), γ = 89.97(2)°, and V = 613.0(2) Å^3 were determined by least-squares fit of 34 reflections with 2θ values between 49.7 and 58.1° with monochromatic Mo$K\alpha$ X-radiation. The cell angles deviate from 90° by less than what was the case for amesite-2H_2. This may mean a lower degree of cation ordering or a different ordering pattern than in amesite-2H_2 because cation ordering was shown by Anderson and Bailey (1981) to be the cause of distortion of the angles. Intensity data were collected by θ-2θ scans in all octants out to 60° with monochromatic Mo$K\alpha$ X-radiation. A total of 3562 intensities were measured, including Friedel equivalents. Absorption correction was attempted by both the semiempirical ψ scan and the analytical shape-correction techniques. Both corrected data sets resulted in several anisotropic displacement parameters that were nonpositive definite during refinement, however, and so the final refinement used intensities without absorption correction. Scan rates were variable from 3 to 30°/min in 2θ with a scan range of 2.0° in 2θ and a background scan range of 0.30°. Two standard reflections were measured every 98 reflections to monitor the electronic and crystal stability. No instability was noted.

To derive initial atomic parameters for refinement, the cation positions for the ideal 2H_2 structure were assumed to be correct, and the positions of the anions were determined from difference electron density maps on the basis of the positions of the heavy atoms. The initial coordinates with disorder of all cations and isotropic displacement factors had a residual R of 26.6%. Initial F^2 least-squares refinement gave cation occupancy values indi-

TABLE 2. Calculated tetrahedral bond lengths (Å) and angles (°)

T1-O1*	1.664(4)	O1*-O3	2.716(4)	O1*-T1-O3	109.23(1)
-O3	1.667(3)	-O4	2.718(4)	-O4	109.49(1)
-O4	1.665(3)	-O5	2.720(4)	-O5	109.30(1)
-O5	1.671(2)	O3-O4	2.737(4)	O3-T1-O4	110.44(1)
Mean	1.667(2)	-O5	2.721(6)	-O5	109.23(1)
		O4-O5	2.718(5)	O4-T1-O5	109.14(1)
		Mean	2.722(2)	Mean	109.47(1)
T2-O2*	1.597(3)	O2*-O3	2.623(4)	O2*-T2-O3	110.21(1)
-O3	1.601(3)	-O4	2.627(4)	-O4	110.22(1)
-O4	1.606(2)	-O5	2.623(4)	-O5	109.72(1)
-O5	1.611(3)	O3-O4	2.603(6)	O3-T2-O4	108.48(1)
Mean	1.604(1)	-O5	2.622(4)	-O5	109.40(1)
		O4-O5	2.616(5)	O4-T2-O5	108.79(1)
		Mean	2.619(2)	Mean	109.47(1)
T11-O11*	1.671(4)	O11*-O33	2.722(4)	O11*-T11-O33	109.14(1)
-O33	1.669(3)	-O44	2.716(4)	-O44	109.10(1)
-O44	1.664(3)	-O55	2.717(4)	-O55	108.96(1)
-O55	1.667(2)	O33-O44	2.734(4)	O33-T11-O44	110.76(1)
Mean	1.668(2)	-O55	2.717(5)	-O55	109.09(1)
		O44-O55	2.724(6)	O44-T11-O55	109.76(1)
		Mean	2.723(2)	Mean	109.47(1)
T22-O22*	1.600(3)	O22*-O33	2.625(4)	O22*-T22-O33	109.90(1)
-O33	1.607(2)	-O44	2.620(4)	-O44	109.87(1)
-O44	1.602(3)	-O55	2.618(4)	-O55	109.66(1)
-O55	1.603(3)	O33-O44	2.601(6)	O33-T22-O44	108.32(1)
Mean	1.603(1)	-O55	2.617(5)	-O55	109.24(1)
		O44-O55	2.623(4)	O44-T22-O55	109.83(1)
		Mean	2.617(2)	Mean	109.47(1)

* Apical O atom.

cating partial ordering of both tetrahedral and octahedral cations. Final refinement utilized the SHELX-93 software least-squares routine with cation occupancies constrained to the chemical analysis of Ranorosoa et al. (1989), unit weights, atomic scattering factors, and anisotropic displacement parameters. Difference electron density maps were essentially featureless at all atomic positions after refinement ceased, and small maxima near the OH groups were taken as the positions of the H^+ protons. The maxima were equivalent to 0.2–0.4 electrons, increasing in the order H2, H4, H33, H3, H44, H22, H11, H1, and were 5–8 times the background variation. The final residual of 5.7% incorporates these H^+ positions, which were not refined.

Table 1 lists the final atomic positions and anisotropic displacement factors. Tables 2 and 3 give calculated bond lengths and angles, with errors calculated by the program ORFFE (Busing et al., 1964). Table 4 summarizes other pertinent structural features, including the refined cation occupancy values. Sheet thicknesses are given in Table 5.

Tetrahedral cation ordering

The degree of partial ordering of $^{[4]}$Si, $^{[4]}$Al, and $^{[4]}$B is the same in both layers. T1 and T11 concentrate Si and Al at the expense of B. The mean T-O bond lengths are 1.667 and 1.668 Å (Table 2), and the average refined occupancy is $Si_{0.61}Al_{0.28}B_{0.11}$ (Table 4). Concentration of the smaller B^{3+} ion [effective ionic radius (IR) of 0.11 Å: Shannon, 1976] in T2 and T22 decreases the mean T-O bonds markedly to 1.604 and 1.603 Å, with an average refined occupancy of $Si_{0.405}Al_{0.145}B_{0.450}$. The latter tetrahedra are more elongate than T1 and T11 (Table 4). B has a greater tendency to concentrate in one tetrahedral site in this structure than do Si or Al, as indicated by the refined occupancies.

Octahedral cation ordering

The degree of partial ordering of Al and Li in octahedral positions is not as great as for the tetrahedral cations. Because of the differences in ionic radii of Al and Li, however, the mean M-O,OH bond lengths differ by as much as do the mean T-O bonds. The small Al (IR = 0.535 Å in sixfold coordination) concentrates slightly in M1, M2, M22, and M33 (refined occupancies of Al = 0.71, 0.71, 0.72, and 0.73 atoms, respectively) to give the shortest mean M-O,OH values (1.960, 1.955, 1.941, and 1.956 Å, respectively). The larger Li (IR = 0.76 Å) concentrates slightly in the two remaining octahedra, M3 and M11 (0.39 and 0.41 atoms relative to an average of 0.28 atoms for the other octahedra), to give the longest mean M-O,OH bond lengths (1.997 and 2.014 Å). The larger, Li-rich octahedra are flattened the most, have the largest RMS variation of internal and external octahedral angles, and have the smallest amounts of counterrotation (Table 4).

Cation ordering pattern

To facilitate the discussion of the approximate directions of ordering paths and positional shifts, the following noncrystallographic axes are used in this and subsequent sections: X_1, X_2, and X_3 refer to a set of three axes situated 0, 120, and 240°, respectively, counterclockwise from **a**, and Z is parallel to **c**. Y_1 refers to an axis situated 90° counterclockwise from X_1. Shifts $+\Delta X$ and $+\Delta Y$ are parallel to X_1 and Y_1, respectively.

In the 2H_2 amesite from Antarctica and the northern

TABLE 3. Calculated octahedral bond lengths (Å) and angles (°)

Octahedron	M1	M2	M3	Octahedron	M11	M22	M33
O1-	1.980(3)	1.981(3)	1.962(3)	O11-	2.093(3)	1.906(3)	1.954(3)
O2-	1.966(3)	1.997(3)	2.053(3)	O22-	2.025(3)	1.981(3)	2.018(3)
OH1-	2.019(3)	1.962(3)	2.002(3)	OH11-	1.981(3)	1.985(3)	1.978(3)
OH2-	1.919(3)	1.926(3)	2.005(3)	OH22-	1.994(3)	1.964(3)	1.873(3)
OH3-	1.965(3)	1.895(3)	1.962(3)	OH33-	1.988(3)	1.888(3)	1.985(3)
OH4-	1.911(3)	1.966(3)	1.995(3)	OH44-	2.003(3)	1.923(3)	1.927(3)
Mean	1.960(1)	1.955(1)	1.997(1)	Mean	2.014(1)	1.941(1)	1.956(1)
Lateral edges		Diagonal edges		Lateral edges		Diagonal edges	
Octahedron M1				**Octahedron M11**			
O1-O2	2.931(7)	O1-OH2	2.603(4)	O11-O22	3.056(7)	O11-OH22	2.657(4)
-OH1	2.913(5)	-OH4	2.625(4)	-OH11	3.042(5)	-OH33	2.688(4)
O2-OH1	2.921(5)	O2-OH3	2.629(4)	O22-OH11	2.993(5)	O22-OH22	2.652(4)
OH2-OH3	2.891(7)	-OH4	2.702(4)	OH22-OH33	3.037(8)	-OH44	2.735(4)
-OH4	2.870(5)	OH1-OH2	2.540(4)	-OH44	2.993(5)	OH11-OH33	2.583(4)
OH3-OH4	2.909(5)	-OH4	2.677(4)	OH33-OH44	2.975(7)	-OH44	2.702(4)
Mean	2.906(2)	Mean	2.629(2)	Mean	3.016(2)	Mean	2.670(2)
Octahedron M2				**Octahedron M22**			
O1-O2	2.896(4)	O1-OH3	2.600(4)	O11-O22	2.817(5)	O11-OH22	2.657(4)
-OH1	2.905(5)	-OH4	2.625(4)	-OH11	2.879(4)	-OH44	2.540(4)
O2-OH1	2.886(7)	O2-OH2	2.697(4)	O22-OH11	2.862(6)	O22-OH33	2.601(4)
OH2-OH3	2.912(4)	-OH3	2.629(4)	OH22-OH33	2.860(4)	-OH44	2.735(4)
-OH4	2.898(5)	OH1-OH2	2.540(4)	-OH44	2.921(6)	OH11-OH22	2.572(4)
OH3-OH4	2.873(6)	-OH4	2.660(4)	OH33-OH44	2.874(5)	-OH33	2.583(4)
Mean	2.895(2)	Mean	2.625(2)	Mean	2.869(2)	Mean	2.615(2)
Octahedron M3				**Octahedron M33**			
O1-O2	2.954(5)	O1-OH2	2.603(4)	O11-O22	2.914(4)	O11-OH33	2.688(4)
-OH1	2.961(7)	-OH3	2.600(4)	-OH11	2.861(6)	-OH44	2.540(4)
O2-OH1	2.975(5)	O2-OH2	2.697(4)	O22-OH11	2.927(4)	O22-OH33	2.601(4)
OH2-OH3	2.978(5)	-OH4	2.702(4)	OH22-OH33	2.885(6)	-OH22	2.652(4)
-OH4	3.014(7)	OH1-OH3	2.677(4)	-OH44	2.869(5)	OH11-OH22	2.572(4)
OH3-OH4	2.998(2)	-OH4	2.660(2)	OH33-OH44	2.933(5)	-OH44	2.702(4)
Mean	2.980(2)	Mean	2.657(2)	Mean	2.898(2)	Mean	2.626(2)

Urals there is one Al-rich tetrahedron and one Al-rich octahedron in each layer, which are located adjacent to one another in projection onto (001), both within each layer and across the interlayer gaps. The locus of Al enrichment in adjacent polyhedra can be traced upward from layer to layer in distinctive patterns, a zigzag line parallel to X_1 in the specimen from Antarctica (Hall and Bailey, 1979) and in counterclockwise spirals along Z in the specimen from the northern Urals (Anderson and Bailey, 1981). Both of these patterns are judged stable because they bring the local source of negative charge ($^{[4]}$Al) on the tetrahedral sheet as close as possible to the local source of positive charge ($^{[6]}$Al) on the octahedral sheet. Sheets of opposite charge are in H-bond contact across the interlayer gap.

The ordering pattern is complicated in manandonite by the presence of two higher charge octahedra in each layer. This causes a hybrid ordering pattern that is a mixture of zigzag lines and spirals. In Figure 1 the solid lines connect adjacent tetrahedra and octahedra within the same layer that are the local sources of negative and positive charges (B-rich tetrahedra and Al-rich octahedra), and dashed lines connect charged octahedra to tetrahedra across the interlayer gap. B-rich T2 is equidistant from Al-rich M1 and M2 in layer 1. One limb of the ordering path of the B- and Al-rich polyhedra progresses upward in the sequence T2-M2-T22-M22-T222 to form a continuous counterclockwise spiral parallel to Z. The other limb progresses upward in the sequence T2-M1-T22-M33-T222 to form a zigzag line parallel to X_1 but also inter-

TABLE 4. Other structural parameters

	T1	T2	T11	T22
Tet. composition	$Si_{0.62}Al_{0.29}B_{0.09}$	$Si_{0.40}Al_{0.14}B_{0.46}$	$Si_{0.60}Al_{0.27}B_{0.13}$	$Si_{0.41}Al_{0.15}B_{0.44}$
Tet. elongation τ (°)	109.34	110.05	109.07	109.81
Tet. rotation α (°)	18.32		18.31	
Basal O corrugation Δz (Å)	−0.025(O4)	−0.074(O33)	+0.079(O44)	

	M1	M2	M3	M11	M22	M33
Oct. composition	$Al_{0.71}Li_{0.29}$	$Al_{0.71}Li_{0.28}\square_{0.01}$	$Al_{0.60}Li_{0.39}\square_{0.01}$	$Al_{0.58}Li_{0.41}\square_{0.01}$	$Al_{0.72}Li_{0.28}$	$Al_{0.73}Li_{0.26}\square_{0.01}$
Oct. counterrotation (°)	0.97	0.85	0.12	0.32	1.50	1.69
Oct. flattening ψ (°)	58.7	58.6	59.3	59.9	58.6	58.9
RMS 15 internal angles	5.67	5.46	6.07	6.50	5.50	5.67
RMS 36 external angles	3.73	3.64	4.21	4.60	3.70	3.83

TABLE 5. Sheet thicknesses (Å)

	Layer 1	Layer 2
Tetrahedral	2.189	2.182
Octahedral	2.024	2.022
Interlayer gap	2.692	2.668
Σ	6.905	6.872

links with the spirals to form other zigzag lines parallel to X_2 and X_3. It is not known whether this hybrid pattern of ordering is less stable than the situation in $2H_2$ amesite that has only a single ordering pattern (spiral or zigzag) as a result of having just one high-charge octahedron in each layer.

H BONDING SYSTEM

Table 6 lists the tilt of each H^+ proton away from the vertical, the angle each OH···H vector makes with $+X_1$, and the H-bond OH-O_b distances. The positions of the H^+ protons are plotted in Figure 2a and 2b for the surface OH groups around one of the inner OH groups of each layer. It can be seen in Figure 2 that all six surface OH···H vectors point almost directly toward their acceptor basal O atoms across the interlayer gap. The tilts from the vertical are 8.9–10.8°, so that the H bonds to the acceptor O atoms are close to straight lines (angles 170.8–179.6°). The distances of the protons from the centers of their associated OH groups (0.900–0.918 Å) are in the expected range (0.90–1.0 Å). The OH-O_b interlayer contact distances are 2.647–2.773 Å, with the four shortest contacts, as well as the one longest, between OH and O_b atoms that are involved in corrugations of the anion surfaces. The tilts from the vertical of the H^+ protons and the OH···H vectors do not appear to be influenced by the adjacent octahedral cations, perhaps because the degree of octahedral ordering is not large.

The two inner OH groups (OH1 and OH11) have similar tilts of their H^+ protons (16°), and the two OH···H vectors are parallel to one another but oppositely directed. Both inner OH groups lie between B-rich tetrahedra

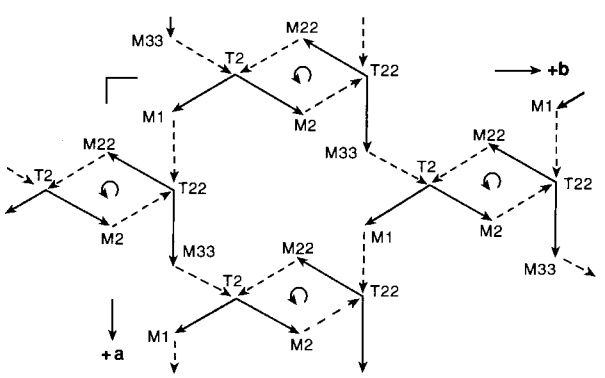

Fig. 1. Cation ordering path between B- and Al-rich polyhedra. Solid lines connect B-rich tetrahedra to two Al-rich octahedra in same layer. Dashed lines connect ordered octahedra to ordered tetrahedra in layer above.

TABLE 6. H distances (Å) and angles (°)

	OH···H	Tilt from vertical	Angle* OH···H to $+X_1$	H-O_b**	OH-O_b	Angle OH···H-O_b
H1	0.867	16.3	−69.4	—	—	—
H2	0.913	9.9	−132.8	1.777(O33)	2.685	172.5
H3	0.909	8.9	+25.9	1.873(O44)	2.773	170.8
H4	0.900	9.6	+138.0	1.790(O55)	2.689	176.7
H11	0.857	16.2	+110.2	—	—	—
H22	0.918	9.2	−62.5	1.817(O5)	2.735	179.6
H33	0.916	10.8	+35.3	1.798(O4)	2.701	174.6
H44	0.910	9.3	−148.4	1.739(O3)	2.647	176.1

* Measured from +X to OH···H vector, clockwise = +.
** Labels of acceptor O atoms given in parentheses.

in the layers above and below, and the directions of their OH···H vectors are parallel to X_3. The opposite directions of the OH···H vectors along X_3 are in accord with the opposite sets of positions occupied by the octahedral cations (I vs. II) in the two layers, but they are aberrant in that H1 points toward Li-rich M3, but H11 points toward Al-rich M33.

STRUCTURAL DISTORTIONS

Because the octahedral sheets of manandonite are Al-rich and those of amesite are Mg-rich, a larger tetrahedral

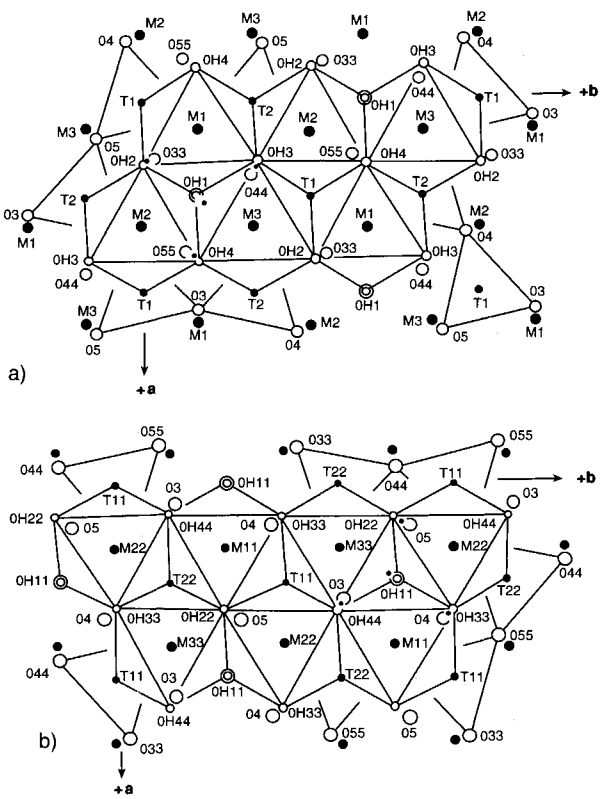

Fig. 2. (a) Layer 1. (b) Layer 2. Basal O atoms of next layer are superimposed on octahedral sheet of each layer. H^+ proton positions shown as small dots for OH groups around one of inner OH groups in each layer.

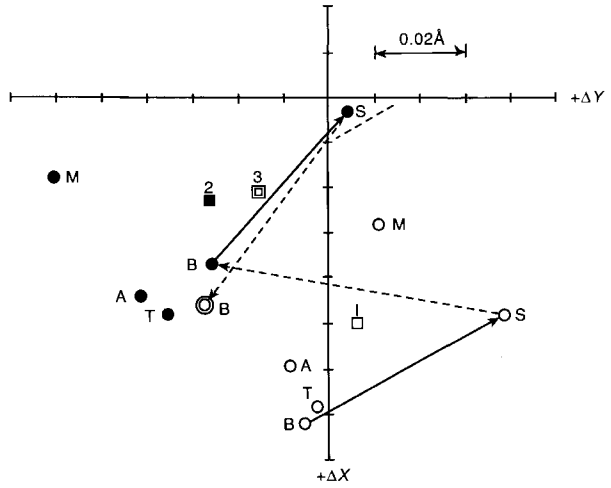

Fig. 3. Displacements of centroids of groups of atoms having similar z heights away from positions in undistorted $2H_2$ structure. Open circles = layer 1; solid circles = layer 2; squares = average of centroids in each layer. Solid lines connect centroids of basal O atoms (B) to those of surface OH molecules (S) in same layer. Dashed lines connect S to B of layer above.

rotation is required in manandonite to reduce the lateral dimensions of the tetrahedral sheet to fit those of the octahedral sheet (α = 18.3° for manandonite vs. 14–15° for amesite). The direction of rotation is the same as in amesite. The basal O atoms move toward both their H-donor OH groups in the layer below and the nearest octahedral cations in their same layer. In layer 1 the apical O atoms of T1 and T2 tilt toward one another in order to form a short lateral edge for the Al-rich M2 octahedron, thereby depressing the bridging basal atom O4 by 0.025 Å relative to O3 and O5. The tilting of O1 and O2 at the same time provides a long lateral edge around the Li-rich octahedron M3 but only provides a torque to the lateral edge around the Al-rich octahedron M1. In layer 2 there are also two smaller Al-rich octahedra (M22 and M33) and one larger octahedron (M11). The apical O atoms of T11 and T22 tilt diagonally away from one another to form a larger lateral edge around M11, elevating the bridging basal atom O44 by 0.079 Å. The diagonal tilts at the same time provide for a smaller lateral edge around M22, depressing O33 by 0.074 Å. This applies a torque to the lateral edge around M33, so that the third bridging basal atom O55 remains at an intermediate z height. The octahedral counterrotations are small (0.1–1.7°). All octahedra are flattened, with the larger Li-rich octahedra flattened more than the smaller Al-rich octahedra (Table 4). In layer 1, OH2 moves down toward OH1 along its shared edge between M1 and M2 to form the shortest of the shared edge lengths (2.540 Å). OH2 is matched with a depressed O33 basal O to form the second shortest H-bond contact (2.685 Å). The shortest H-bond contact (2.647 Å) is between an elevated OH44 and a depressed O3 between layers 2 and 3. The longest octahedral shared edges involve the apical O atoms in the small B-rich tetrahedra T2 and T22.

The displacements, in projection onto (001), of the different atomic planes relative to the ideal atomic coordinates of the undistorted $P6_3$ symmetry of the $2H_2$ structure can be determined by calculating the ΔX and ΔY displacements of the centroids (averages of the Cartesian coordinates) for groups of atoms having similar z heights, e.g., the three M cations or the three basal O atoms). Figure 3 shows that the centroids of all the atoms are displaced (actual minus ideal) along +X relative to the coordinate origin, but by differing amounts. Within each layer there is a displacement of about 0.05 Å of the surface OH groups (S in Fig. 3) relative to the basal O atoms (B) along $+X_2$ (solid lines in Fig. 3). The displacements from the surface OH groups across the interlayer gap (dashed lines) to the basal O atoms of the next layer are about 0.06 Å, but in different directions because of the different sets of octahedral positions occupied in the two layers (II vs. I). The centroid for the octahedral cations (M) in layer 2 is displaced considerably along $-Y_1$. M11 (Li-rich) is displaced much more than Al-rich M22 and M33 (0.094 Å relative to 0.040 and 0.045 Å, respectively), but these points are not shown in Figure 3.

The average of the centroids of layer 2 (solid square) is displaced by 0.04 Å along $+X_3$ relative to the average of the centroids of layer 1 (open square), and the average of the centroids in layer 3 (double open square) comes back 0.01 Å along $+Y_1$. The position of this latter average point relative to that of layer 1 represents the offset due to the deviation of the α and β angles from 90°. A diagram of centroid displacements illustrates the complex interactions caused by the ordered distribution of cations of different size and charge. The rotations, tilts, attractions, and repulsions leading to the most stable structure affect certain groups of atoms more than others, as evident in Figure 3.

The anisotropic vibrational ellipsoids for manandonite are typical for those of trioctahedral 1:1 structures. The major axes for the ellipsoids for all the cations, apical O atoms, and inner OH groups are parallel to Z. The basal O atoms vibrate most parallel to (001) in a direction normal to their Si-O-Si bonds. The surface OH groups vibrate most toward the basal O atoms to which they form H bonds.

Acknowledgments

This research was supported in part by NSF grant EAR-8614868 and in part by grant 17966-AC2-C from the Petroleum Research Fund, administered by the American Chemical Society. We are indebted to A.-M. Fransolet for supplying us with the specimen under study, to the Department of Chemistry, University of Wisconsin–Madison, for the use of their diffraction facilities, and to Randy Hayashi for technical assistance.

References cited

Anderson, C.S., and Bailey, S.W. (1981) A new cation ordering pattern in amesite-$2H_2$. American Mineralogist, 66, 185–195.

Bailey, S.W. (1969) Polytypism of trioctahedral 1:1 layer silicates. Clays and Clay Minerals, 17, 155–171.

Busing, W.R., Martin, K.O., and Levy, H.A. (1964) OR FFE, a Fortran crystallographic function and error program. Oak Ridge National Laboratory Technical Manual 306.

Caillère, S., Hénin, S., and Rautureau, M. (1982) Minéralogie des Argiles, vol. 2: Classification et nomenclature (2nd edition), 189 p. Masson, Paris.

Fleischer, M. (1987) Glossary of mineral species (5th edition), 227 p. The Mineralogical Record, Inc., Tucson, Arizona.

Frank-Kamenetsky, V.A. (1960) A crystallochemical classification of simple and interstratified clay minerals. Clay Minerals Bulletin, 4, 161–172.

Hall, S.H., and Bailey, S.W. (1979) Cation ordering pattern in amesite. Clays and Clay Minerals, 27, 241–247.

Hawthorne, F.C., and Černý, P. (1982) The mica group. In Short course in granitic pegmatites in science and industry, p. 63–98. Mineralogical Association of Canada, Winnipeg, Manitoba, Canada.

Lacroix, A. (1912) Sur une nouvelle espèce minérale (manandonite) des pegmatites de Madagascar. Bulletin de la Société français de Minéralogie, 35, 223–226.

——— (1922) Minéralogie de Madagascar, Tome I. Géologie, Descriptive Minéralogie, p. 481–482. Librairie Maritime Coloniale, Paris.

London, D., and Burt, D.M. (1982) Lithium minerals in pegmatites. In Short course in granitic pegmatites in science and industry, p. 99–103. Mineralogical Association of Canada, Winnipeg, Manitoba, Canada.

Ranorosoa, N., Fontan, F., and Fransolet, A.-M. (1989) Rediscovery of manandonite in the Sahatany Valley, Madagascar. European Journal of Mineralogy, 1, 633–638.

Sahama, Th.G., von Knorring, O., and Lethinen, M. (1968) Cookeite from the Muaine pegmatite, Zamezia, Mozambique. Lithos, 1, 12–19.

Shannon, R.D. (1976) Revised effective ionic radii and systematic studies of interatomic distance in halides and chalcogenides. Acta Crystallographica, A32, 751–767.

Strunz, H. (1957) Bor und Beryllium in Phyllosilikaten. Rendiconti della Società Italiana di Mineralogia e Petrologia, 13, 372.

Manuscript received June 6, 1994
Manuscript accepted December 6, 1994